

Slightly Frequency-Shifted Reference Ultra-Wideband (UWB) Radio

Dennis L. Goeckel and Qu Zhang
University of Massachusetts - Amherst

Abstract

A promising ultra-wideband (UWB) radio technique being widely considered for low data rate applications, such as those often encountered in sensor networks, is the transmitted reference (TR) UWB scheme. However, the standard TR-UWB scheme, while often motivated by the simplicity of its receiver, is still dogged by implementation concerns. In particular, the receiver requires an extremely wideband delay element, which is difficult to incorporate into low-power integrated systems. In this paper, a transmitted-reference scheme is proposed in which the separation between the data and reference signals, rather than being a time delay, is a slow rotation over the symbol interval. This provides a (slightly) frequency-shifted reference that, while orthogonal to the data-bearing pulse, still goes through a nearly equal channel. A detailed analysis of the proposed scheme is provided. Simulation results demonstrate the expected result that frequency shifting of the reference in the proposed manner is not effective for high data rate systems that experience appreciable intersymbol interference. However, for the targeted low to moderate data rate applications, numerical results demonstrate that the proposed system not only achieves the primary goal of providing a much simpler receiver architecture, but also that it outperforms the standard TR-UWB system.

Keywords: Communication system signaling, multipath channels, receivers.

Corresponding Author

Dennis Goeckel
Electrical and Computer Engineering
University of Massachusetts
100 Natural Resources Road
Amherst, MA 01003-9292
Tel:(413) 545-3514
Fax:(413) 545-4611
Email: goeckel@ecs.umass.edu

Qu Zhang
Electrical and Computer Engineering
University of Massachusetts
100 Natural Resources Road
Amherst, MA 01003-9292
Tel: (413) 545-0963
FAX: (413) 545-4611
qzh@acad.umass.edu

¹This paper is based in part upon work supported by the Army Research Office under Contract DAAD10-01-1-0477 and a grant from M/A-COM, Inc., and employed equipment obtained under National Science Foundation Grant EIA-0080119.

²A preliminary version of this work appeared at the 2005 Military Communications Conference, Atlantic City, New Jersey.

1 Introduction

Ultra-wideband (UWB) communication systems have emerged as a potential alternative to conventional communication systems for short-range, low-power wireless applications. From a regulatory standpoint, the extremely low power density of UWB communications has motivated the federal communications commission (FCC) of the United States to allow UWB systems to operate in bands already allocated to other radios, thus helping to solve the frequency allocation problem that often inhibits high data rate wireless communication systems. From a technical standpoint, the extremely wide bandwidth offers a number of *potential* advantages for wireless transmission versus narrowband alternatives, including the ability to carry very high data rates, an extremely large amount of frequency diversity to combat multipath fading, and significant mitigation of both multi-user and non-system interference.

However, the large bandwidth of UWB systems can also make receiver design very difficult in traditional UWB systems that employ either antipodal or pulse-position modulation with extremely short pulses [1]. For simple low-power UWB receivers, digitization of the entire signaling bandwidth (e.g. 7 GHz) is far from being realizable in current analog-to-digital (A/D) conversion technology [2]. Hence, many UWB receivers that are largely digital have some number of analog correlators to collect signal energy in a front-end rake receiver type architecture [3]. Unfortunately, due to the many resolvable paths in the standard fading environment, efficient energy collection in such an architecture can be costly in terms of circuit area and power, and, even if allowable from a circuit complexity standpoint, can present problems in terms of channel estimation [4]. These implementation problems have been a large motivation for the industry shift away from traditional impulsive UWB or direct-sequence UWB to the multiband UWB approach for short-range high data rate applications [5].

One method of addressing the receiver complexity problems in the impulse-based UWB system, particularly in low data rate systems, is through the use of the transmitted reference (TR) UWB system [6]-[12]. In the TR-UWB system, each frame consists of two pulses. The first is a “reference pulse”, which has a fixed polarity. The second, which follows at some known delay D ,

is a “data pulse” whose polarity indicates the data bit. In low data rate systems, these two pulses are then repeated over many frames to allow energy aggregation at the receiver. In the standard receiver configuration [6], the received signal is correlated against a version of itself delayed by D to produce the decision variable. This TR-UWB architecture has the attractive property of achieving full multipath energy collection, since the reference arm of the receiver provides a perfect (but, unfortunately, noisy) template to which to match the data pulse. In exchange for the ostensibly simple receiver, TR-UWB systems are generally viewed as inferior to standard UWB systems in error performance due to the “noise cross noise” terms arising in the receiver. However, some recent work has suggested that standard UWB systems (e.g. antipodal systems) incur a similar performance loss as that observed in the TR-UWB system when errors in the channel estimates required to determine the combining coefficients for the rake receiver are considered [13].

Because of the promise of the TR-UWB architecture, particularly in providing a simple receiver design for a UWB system, it is currently being considered for a number of low data rate applications. However, despite the simplicity at first glance of the TR-UWB receiver, implementation can be daunting. In particular, the delay element, which must handle a wideband analog signal, is difficult to build in the low-power integrated fashion desirable for the TR-UWB receiver [14, 15]. In fact, the difficult design of such a delay element (or, equivalently, a filter with exact linear phase) is oft-cited as one of the great drawbacks of analog circuits [16, pg. 44]. For design simplicity, [17] implemented the delay using the appropriate length of coaxial cable (e.g. 20 feet of cable for 20 ns of delay), which clearly is infeasible for low-power integrated receivers. Furthermore, many of the improved versions of the TR-UWB system proffered in the literature further exacerbate this problem by needing to extend this delay [7, 9, 10].

The main motivation here is to prescribe an effective TR-UWB system that avoids the delay element in the receiver for standard TR-UWB. Because the implementation of a frequency translation of a wideband signal is much simpler than the delay of the same signal, the technique considered here is to employ a very carefully selected frequency-translated reference; in other words, the reference is translated in frequency (rather than time) to be orthogonal to the data-bearing signal. The

key observation that leads to the solution proffered here is to recognize that this orthogonality of the reference and data signals does not have to be enforced over each frame period but rather over a symbol period. Hence, a frequency offset between the reference impulse train and data impulse train is prescribed that is only the inverse of the symbol period. For low data rate applications (say, for now, less than 100 kbits/s), this frequency shift is well below the frequency coherence of the channel, and, hence, as desired, the reference serves as a suitable (albeit not perfect, because it is not only noisy but slightly shifted in frequency) reference for the data-bearing signal. In this paper, this slightly frequency-shifted reference UWB system is introduced and characterized.

The contributions of this paper are potentially significant to the implementation of UWB systems. These contributions include: (1) the recognition that a properly frequency-shifted reference can remove the requirement for a delay element at the receiver in TR-UWB systems, (2) the prescription of a scheme that provides such a reference for low to moderate data rate applications, and (3) the performance characterization of the proposed scheme.

2 Development of the Proposed Scheme

Throughout this paper, a baseband UWB system will be assumed. Since low data rate applications are targeted, a symbol interval $T_s = N_f T_f$ consists of $N_f \gg 1$ frames, each of duration T_f and carrying one data pulse of the UWB transmission. In the standard TR-UWB system [6], the transmitted signal for the l^{th} symbol is given by:

$$x(t) = \sum_{k=0}^{N_f-1} \left(\sqrt{E_s/2} p(t - lT_s - kT_f) + (-1)^{b_l} \sqrt{E_s/2} p(t - lT_s - kT_f - D) \right) \quad (1)$$

where E_s is the transmitted energy per symbol period, $b_l \in \{0, 1\}$ is the information bit to be transmitted across the channel during the l^{th} symbol period, and $p(\cdot)$ is a normalized UWB pulse shape with energy $\frac{1}{N_f}$, approximate bandwidth W , and approximate support on $[0, T_p]$ with $T_p \ll T_f$.

Per Section 1, the TR-UWB receiver requires the ability to delay the wideband received signal by some amount D (generally tens of nanoseconds), which can be difficult in low-power integrated receivers. Hence, a method is sought to obtain an orthogonal reference that can be more

easily recovered by the receiver. Per Section 1, frequency translation of wideband signals can be readily accomplished with a mixer. The work of [18] put forward a frequency-translated reference as an example of a non-standard TR-UWB system covered by their generalized framework for TR-UWB. However, that example immediately illustrates the main perils of this avenue of approach. Since the data pulse must go through approximately the same channel as the reference pulse, frequency orthogonality obtained by simply shifting the data pulse is ineffective, because the frequency separation between the pulses exceeds the coherence frequency of any reasonable fading channel. This is addressed in [18] by restricting the reference pulse shape to be one whose frequency response consists of the union of a large number of disjoint regions, with gaps in between these disjoint regions for the data signal's frequency response. However, the construction of such a pulse is complicated, and, hence, we seek a solution that does not require modification of the basic UWB pulse shape.

The key observation is to note that the frequency shift of the data signal relative to the reference signal need not be accomplished over a frame but rather over a symbol interval, which, in contrast to [18], allows *significant* overlap of the frequency bands which the data-bearing and reference signal occupy. To develop this frequency-shifted reference UWB (FSR-UWB) approach, define a basic template signal $u(t)$, which consists of N_f unmodulated UWB pulses with a “standard” UWB pulse shape $p(\cdot)$, as $u(t) = \sum_{k=0}^{N_f-1} p(t - kT_f)$. We note, in passing, that the regular structure of the pulses in $u(t)$ is not necessary for this approach to work (i.e. the pulses can easily be dithered if desired to improve spectral properties). The reference waveform is set to be a scaled version of $u(t)$, and the data waveform is set as a frequency shifted version of this signal that is approximately orthogonal to it *over the symbol interval* for large N_f . Thus, defining $f_0 = \frac{1}{T_s}$ as the frequency shift of the data signal relative to the reference, the transmitted signal over interval $[lT_s, (l+1)T_s]$ is given by:

$$x(t) = \sqrt{E_r}u(t - lT_s) + \sqrt{2E_d}(-1)^{b_l}u(t - lT_s) \cos(2\pi f_0 t) \quad (2)$$

where E_r and E_d are the energy per symbol invested in the reference signal and the data-bearing signal, respectively.

Figure 1(a) shows the natural conversion of the standard TR-UWB receiver to that for the proposed system, but, recognizing that multiplication is commutative results in the receiver in Figure 1(b). The latter is useful not only for analysis, but also for interpretation and relation of the scheme to other potential schemes, such as on-off keying with energy detection. Furthermore, it suggests the placement of the technique in the broader history of communication theory (outside of the context of modern UWB systems). In particular, the scheme can be viewed as using the lowpass signal

$$\sum_{l=-\infty}^{\infty} (\sqrt{E_r} + \sqrt{2E_d}(-1)^{b_l}) d(t - lT_s) \cos(2\pi f_0 t), \quad (3)$$

where $d(\cdot)$ is a rectangular pulse of duration T_s , to amplitude modulate (AM) an infinite sequence of short-duration pulses. The standard receiver for a conventional AM system, where the loss of sign on the modulating signal is acceptable (as is the case here, as well), is an envelope detector[19, pg. 309]. Since operation of the UWB system proposed here is at baseband, there is no unknown phase component, and thus a square-law device followed by a low-pass filter, which is the analog to the envelope detector in the standard AM system, can be employed. When the low-pass filter is combined with the lowpass data demodulation circuit, the architecture in Figure 1(b) results.

To understand the precise operation of the proposed receiver, let $r(t) = x(t)$ (i.e. ignore the noise for now) and, without loss of generality, consider the receiver output for the first bit (b_0):

$$\begin{aligned} r_0 &= \int_0^{T_s} x^2(t) \sqrt{2} \cos(2\pi f_0 t) dt \\ &= \sqrt{2} E_r \int_0^{T_s} u^2(t) \cos(2\pi f_0 t) dt + 4\sqrt{E_r E_d} (-1)^{b_0} \int_0^{T_s} u^2(t) \cos^2(2\pi f_0 t) dt \\ &\quad + 2\sqrt{2} E_d \int_0^{T_s} u^2(t) \cos^3(2\pi f_0 t) dt \end{aligned} \quad (4)$$

Throughout this paper, there will be many integrals of the form: $\int_0^{T_s} u^2(t) g(t) dt$ where $g(t)$ is a narrowband signal, and $u(t)$, as defined above, is a sequence of N_f short pulses equally spaced over T_s . Consider:

$$\begin{aligned} \int_0^{T_s} u^2(t) g(t) dt &= \sum_{k=0}^{N_f-1} \int_0^{T_s} p^2(t - kT_f) g(t) dt \approx \sum_{k=0}^{N_f-1} \int_0^{T_s} p^2(t - kT_f) g(kT_f) dt = \frac{1}{N_f} \sum_{k=0}^{N_f-1} g(kT_f) \\ &\approx \frac{1}{T_s} \int_0^{T_s} g(t) dt \end{aligned} \quad (5)$$

where the first equality is due to the orthogonality of pulses from different frames, the first approximation arises because the narrowband signal $g(\cdot)$ can be approximated as constant over the small interval T_p , and the last approximation comes from the observation that $N_f \gg 1$ for the applications of interest and the definition of the Riemann integral. Using basic trigonometric identities and this simplification in (4) yields $r_0 = 2\sqrt{E_r E_d}(-1)^{b_0}$. The partitioning of the symbol energy E_s between E_r and E_d should be done to optimize the output signal-to-noise ratio (SNR). However, as will be demonstrated later, the “noise cross noise” terms will dominate receiver performance at the error rates of interest, and thus a partitioning to maximize this noiseless r_0 is sufficient and will greatly simplify notation. Hence, subject to $E_d + E_r = E_s$, $E_r E_d = E_r(E_s - E_r)$ must be maximized. Differentiating $E_r(E_s - E_r)$ with respect to E_r and equating the result to zero reveals that the maximum is achieved by setting $E_r = E_d = \frac{E_s}{2}$; hence, $r_0 = (-1)^{b_0} E_s$.

3 Performance Analysis

For low data rate UWB systems, simulation is difficult, since there can be many orders of magnitude between the symbol period and the sampling rate of an accurate simulator. Hence, an accurate performance analysis is critical.

3.1 Additive White Gaussian Noise (AWGN)

The received signal is given by $\tilde{r}(t) = x(t) + \tilde{n}(t)$, where $\tilde{n}(t)$ is a zero-mean Gaussian random process with (two-sided) power spectral density $S_{\tilde{n}}(f) = \frac{N_0}{2}$. Assuming that the lowpass filter at the front end of the receiver passes the transmitted signal without distortion, the signal at its output is given by $r(t) = x(t) + n(t)$, where $n(t)$ is a zero-mean Gaussian random process with power spectral density $S_n(f) = |H(f)|^2 \frac{N_0}{2}$ and $H(f)$ is the frequency response of the front-end filter.

For the first bit b_0 , the integrator output r_0 can be expressed as:

$$\begin{aligned} r_0 &= \int_0^{T_s} r^2(t) \sqrt{2} \cos(2\pi f_0 t) dt \\ &= \int_0^{T_s} (x(t) + n(t))^2 \sqrt{2} \cos(2\pi f_0 t) dt \end{aligned}$$

$$= (-1)^{b_0} E_s + 2\sqrt{2} \int_0^{T_s} x(t)n(t) \cos(2\pi f_0 t) dt + \sqrt{2} \int_0^{T_s} n^2(t) \cos(2\pi f_0 t) dt \quad (6)$$

The latter two terms, which will be denoted the “noise terms”, will be grouped into a single random variable n_0 . Following the argument for the standard TR-UWB system [6], it is straightforward to establish that n_0 is approximately Gaussian. Hence, only its mean and variance need to be calculated to complete the performance characterization.

The mean of n_0 is given by:

$$\begin{aligned} E[n_0] &= 2\sqrt{2} \int_0^{T_s} E[x(t)]E[n(t)] \cos(2\pi f_0 t) dt + \sqrt{2} \int_0^{T_s} E[n^2(t)] \cos(2\pi f_0 t) dt \\ &= \sqrt{2} \int_0^{T_s} R_n(0) \cos(2\pi f_0 t) dt \\ &= 0, \end{aligned} \quad (7)$$

where $R_n(\cdot)$ denotes the autocorrelation function of $n(t)$, and the variance of n_0 is given by:

$$\begin{aligned} E[n_0^2] &= E \left[\left(2\sqrt{2} \int_0^{T_s} x(t)n(t) \cos(2\pi f_0 t) dt + \sqrt{2} \int_0^{T_s} n^2(t) \cos(2\pi f_0 t) dt \right)^2 \right] \\ &= E \left[\left(2\sqrt{2} \int_0^{T_s} x(t)n(t) \cos(2\pi f_0 t) dt \right)^2 \right] + E \left[\left(\sqrt{2} \int_0^{T_s} n^2(t) \cos(2\pi f_0 t) dt \right)^2 \right] \quad (8) \\ &= \frac{5}{2} E_s N_0 + T_s N_0^2 W \quad (9) \end{aligned}$$

where the last line comes from the detailed analysis in Appendix A. The bit error probability of the proposed system on AWGN channels then follows easily as:

$$P_{FSR-UWB,AWGN} = Q \left(\frac{E_s}{\sqrt{\frac{5}{2} E_s N_0 + T_s N_0^2 W}} \right) \quad (10)$$

The bit error probability of standard TR-UWB on an AWGN channel is [6, 12]:

$$P_{TR-UWB,AWGN} = Q \left(\frac{E_s}{\sqrt{4E_s N_0 + 2T_s N_0^2 W}} \right) \quad (11)$$

Assuming that the two systems employ the same parameters would lead to the conclusion that the proposed system demonstrates a 1.5 to 2.0 dB gain over the standard TR-UWB system. However, judgments on the applicability of the two systems should be reserved until the overall system

constraints of interest (e.g. data rate and peak pulse energy) are fixed, and then the performance of the two systems - each with its appropriate parameters - can be compared. This comparison is carried out in Section 4 below.

3.2 Multipath Fading

In standard TR-UWB systems with no inter-frame and interpulse interference, the probability of error conditioned on the multipath fading channel is the same as in AWGN except with a modified pulse shape. However, this is not true for the proposed system, since there is a loss incurred due to the reference pulse traveling through a slightly different (although greatly overlapping) frequency band than the data pulse.

For the multipath fading channel, the received signal is denoted by: $\tilde{r}(t) = h(t) * x(t) + \tilde{n}(t)$, where $h(t)$ is the channel impulse response. Here, a discrete path model is assumed for the channel; hence, $h(t)$ can be written as:

$$h(t) = \sum_{l=0}^{L-1} h_l \delta(t - \tau_l) \quad (12)$$

where L is the number of paths, h_l is the amplitude of the l^{th} path, $\delta(\cdot)$ is the Dirac delta function, and τ_l is the delay of the l^{th} path.

The noise analysis of the previous section still holds with the modified pulse shape $h(t) * p(t)$. However, the desired signal component changes as follows (neglecting inter-frame interference):

$$\begin{aligned} r_0 &= \int_0^{T_s} \left(\sum_{l=0}^{L-1} h_l x(t - \tau_l) \right)^2 \sqrt{2} \cos(2\pi f_0 t) dt \\ &= \sqrt{2} \sum_{l=0}^{L-1} \sum_{m=0}^{L-1} h_l h_m \int_0^{T_s} x(t - \tau_l) x(t - \tau_m) \cos(2\pi f_0 t) dt \\ &= \sqrt{2} \sum_{l=0}^{L-1} \sum_{m=0}^{L-1} h_l h_m \int_0^{T_s} u(t - \tau_l) u(t - \tau_m) \left(\sqrt{\frac{E_s}{2}} + \sqrt{E_s} (-1)^{b_0} \cos(2\pi f_0 (t - \tau_l)) \right) \\ &\quad \left(\sqrt{\frac{E_s}{2}} + \sqrt{E_s} (-1)^{b_0} \cos(2\pi f_0 (t - \tau_m)) \right) \cos(2\pi f_0 t) dt \\ &= \sqrt{2} \sum_{l=0}^{L-1} \sum_{m=0}^{L-1} h_l h_m \int_0^{T_s} \sum_{k=0}^{N_f-1} p(t - kT_f - \tau_l) \sum_{n=0}^{N_f-1} p(t - nT_f - \tau_m) \end{aligned}$$

$$\begin{aligned}
& \left(\frac{E_s}{2} + \frac{E_s}{\sqrt{2}}(-1)^{b_0} \cos(2\pi f_0(t - \tau_l)) \right. \\
& \left. + \frac{E_s}{\sqrt{2}}(-1)^{b_0} \cos(2\pi f_0(t - \tau_m)) + E_s \cos(2\pi f_0(t - \tau_l)) \cos(2\pi f_0(t - \tau_m)) \right) \cos(2\pi f_0 t) \\
\approx & (-1)^{b_0} E_s \sum_{l=0}^{L-1} \sum_{m=0}^{L-1} h_l h_m \rho(|\tau_m - \tau_l|) \left(\frac{1}{2} \cos(2\pi f_0 \tau_l) + \frac{1}{2} \cos(2\pi f_0 \tau_m) \right) \quad (13)
\end{aligned}$$

where $\rho(|\tau_m - \tau_l|)$ denotes the correlation of $u(t - \tau_m)$ and $u(t - \tau_l)$:

$$\rho(|\tau_m - \tau_l|) \triangleq N_f \int_0^{T_f} p(t - \tau_m) p(t - \tau_l) dt. \quad (14)$$

In the case when distinct paths are orthogonal (such as $|\tau_m - \tau_l| > T_p, \forall m \neq l$), r_0 reduces to:

$$r_0 = (-1)^{b_0} E_s \sum_{l=0}^{L-1} h_l^2 \cos(2\pi f_0 \tau_l), \quad (15)$$

and the probability of error for the proposed system operating over a multipath fading channel is:

$$P_{FSR-UWB,MP} = E_h \left[Q \left(\frac{E_s \sum_{l=0}^{L-1} h_l^2 \cos(2\pi f_0 \tau_l)}{\sqrt{\frac{5}{2} E_s N_0 \sum_{l=0}^{L-1} h_l^2 + T_s N_0^2 W}} \right) \right], \quad (16)$$

thus establishing a mathematical justification for using the smallest frequency shift possible between the reference and data signals. For the standard TR-UWB system, one obtains:

$$P_{TR-UWB,MP} = E_h \left[Q \left(\frac{E_s \sum_{l=0}^{L-1} h_l^2}{\sqrt{4 E_s N_0 \sum_{l=0}^{L-1} h_l^2 + 2 T_s N_0^2 W}} \right) \right] \quad (17)$$

where $E_h[\cdot]$ is the expectation over the channel impulse response.

4 Numerical Results

4.1 Synchronization

As with many communication systems, the synchronization values that potentially must be estimated include any oscillator mismatch between the transmit and receive oscillators (in this case, of frequency f_0) and the symbol timing. Fortunately, the relatively low frequency $f_0 = \frac{1}{T_s}$ is easily matched within the necessary tolerances between the transmitter and receiver. More critical, as is the case with most UWB systems (see [20] and references therein), is timing synchronization. In the FSR-UWB system, the key is the ability to set the symbol timing δ as shown in Figure 2.

One method of demonstrating the system's ability to be synchronized is to show that there exists a quantity based on the output of Figure 2 that, when minimized as a function of δ , yields the proper symbol timing. Then, adaptive algorithms can be employed to minimize such quantity and obtain the proper timing.

The receiver of Figure 2 can be used to specify a frequency domain version of the “dirty template” method of [13], where the one-symbol delay element of [13] is replaced with a mixer. For $\delta \in [0, T_s]$, define the receiver output as

$$\Lambda(\delta) = \int_{\delta}^{T_s+\delta} r^2(t) \sqrt{2} \cos(2\pi f_0(t - \delta)) dt = \Lambda_s(\delta) + \Lambda_n(\delta) \quad (18)$$

where

$$\Lambda_s(\delta) = \int_{\delta}^{T_s+\delta} (h(t) * x(t))^2 \sqrt{2} \cos(2\pi f_0(t - \delta)) dt \quad (19)$$

is the received signal component, and

$$\Lambda_n(\delta) = \int_{\delta}^{T_s+\delta} (n^2(t) + 2(h(t) * x(t))n(t)) \sqrt{2} \cos(2\pi f_0(t - \delta)) dt \quad (20)$$

is the (approximately Gaussian) noise component.

For AWGN channels, simple trigonometric identities can be employed to show that, for any given δ , $\Lambda_s(\delta)$ has zero mean and variance given by

$$E[\Lambda_s^2(\delta)] = E_s^2 \left[\frac{1}{2} + \frac{1}{4\pi^2} - \frac{\delta}{T_s} + \frac{\delta^2}{T_s^2} \right] \quad (21)$$

$$+ E_s^2 \left[\left(\frac{1}{2} - \frac{1}{4\pi^2} - \frac{\delta}{T_s} + \frac{\delta^2}{T_s^2} \right) \cos(4\pi f_0 \delta) + \frac{1}{2\pi} \left(\frac{2\delta}{T_s} - 1 \right) \sin(4\pi f_0 \delta) \right], \quad (22)$$

which contains a low-frequency term (21) that has two peaks at $\delta = 0$ and $\delta = T_s$; and a term (22) of frequency $2f_0$. The noise term $\Lambda_n(\delta)$ can be shown to have zero mean and variance given by

$$E[\Lambda_n^2(\delta)] = T_s W N_0^2 + 2E_s N_0 + \frac{1}{2} \cos(4\pi f_0 \delta) E_s N_0, \quad (23)$$

which also contains a low-frequency term that does not depend on δ , and a term of frequency $2f_0$. Moreover, it can be shown that $\Lambda_s(\delta)$ and $\Lambda_n(\delta)$ are uncorrelated. Therefore, $\Lambda(\delta)$ has zero mean and variance

$$E[\Lambda^2(\delta)] = E[\Lambda_s^2(\delta)] + E[\Lambda_n^2(\delta)]. \quad (24)$$

In a multipath environment, it can be shown similarly that (24) still holds, where

$$\begin{aligned}
E\{\Lambda_s^2(\delta)\} &= E_h \left[E_s^2 \sum_{n=0}^{L-1} \sum_{m=0}^{L-1} h_m h_n \right. \\
&\quad \left[\left(\left(1 - \frac{\delta}{T_s}\right) \cos(2\pi f_0(\delta - \tau_m)) - \frac{\sin(2\pi f_0\delta) \cos(2\pi f_0\tau_m)}{2\pi} \right) \right. \\
&\quad \left(\left(1 - \frac{\delta}{T_s}\right) \cos(2\pi f_0(\delta - \tau_n)) - \frac{\sin(2\pi f_0\delta) \cos(2\pi f_0\tau_n)}{2\pi} \right) \\
&\quad + \left(\frac{\delta}{T_s} \cos(2\pi f_0(\delta - \tau_m)) + \frac{\sin(2\pi f_0\delta) \cos(2\pi f_0\tau_m)}{2\pi} \right) \\
&\quad \left. \left. + \left(\frac{\delta}{T_s} \cos(2\pi f_0(\delta - \tau_n)) + \frac{\sin(2\pi f_0\delta) \cos(2\pi f_0\tau_n)}{2\pi} \right) \right] \right],
\end{aligned}$$

and

$$E[\Lambda_n^2(\delta)] = E_h \left[T_s W N_0^2 + \left(2E_s N_0 + \frac{1}{2} \cos(4\pi f_0\delta) E_s N_0 \right) \sum_{l=0}^{L-1} h_l^2 \right]. \quad (25)$$

where $E_h[\cdot]$ denotes expectation over the channel impulse response.

An example of $E[\Lambda^2(\delta)]$ is shown in Fig. 3 for each of an AWGN and a multipath fading channel. The signal-to-noise ratio is 24 dB, the pulse shape $p(t)$ is the second derivative of Gaussian with a zero-to-zero pulse width of 1.0 ns, and the bandwidth of the front end filter is 2.5 GHz (one-sided). Each symbol period consists of 100 frames, each of length 40 ns. The multipath fading channel consists of 20 discrete multipaths spaced at 2 ns, and with power drawn from the exponential profile $\frac{1}{\bar{\tau}} e^{-\frac{t}{\bar{\tau}}}$, with $\bar{\tau} = 15$ ns. As the figure shows, $E[\Lambda^2(\delta)]$ has two maxima on $[0, T_s]$ at $\delta = 0$ and $\delta = T_s$ - either of which corresponds to perfect timing. This suggests a receiver as shown in Figure 2 that scans $\delta \in [0, T_s]$ at some small resolution, calculating an empirical version of $E[\Lambda^2(\delta)]$ for each δ , and choosing the argument of the maximum. In reality, this would likely be accomplished via an adaptive algorithm with $E[\Lambda^2(\delta)]$ as the metric to be minimized and a slight modification to avoid the peak at $\delta = 0.5T_s$.

The simple timing synchronization algorithm proffered above, which, very importantly, does not require the delay of a wideband signal, is not intended to be a major contribution of this work. The purpose is to establish that the proposed system can be synchronized without having to sacrifice the simplicity of the receiver. Throughout the remainder of the numerical results and paper, it will be assumed that the system synchronization is perfect.

4.2 Performance Plots

For all of the results presented, the pulse shape is the second derivative of Gaussian with a zero-to-zero pulse width of 0.25 ns. The noise bandwidth, corresponding to that of the front end filter, is 10.0 GHz (one-sided).

Before performing the important comparison between TR-UWB and FSR-UWB, first the accuracy of the formulas derived in this paper are checked for AWGN and multipath fading channels. To reflect current system constraints (and to match the detailed comparison results below) the bit error performance is plotted versus the peak energy per UWB pulse (defined as E_p) rather than the average symbol energy. Figure 4 displays (10) and the simulated performance of the FSR-UWB system on an AWGN channel for various data rates and a fixed frame time of $T_f = 40$ ns. The analytical results agree very well with the simulation results except for the data rate $R_b = 12.5$ Mbits/s. Recognizing that $R_b = 1/(N_f T_f)$, the $R_b = 12.5$ Mbits/s curve corresponds to $N_f = 2$ frames per symbol, where the approximations made throughout this paper for performance characterization break down. However, for the targeted low to moderate data rate applications, the conclusion is that the approximations made in this paper for the derivation of (10), ranging from those made in (5) to those made in the appendix, are valid.

Next, performance of the FSR-UWB system in a multipath fading environment is considered to both verify the accuracy of (16) and to study at what (high) data rates the system performance starts to degrade due to the frequency offset f_0 between the reference and data signals. For the simulation results over multipath channels, channel models from the IEEE 802.15.4a standardization effort are employed [22]. Figure 5 shows analytical and simulation results at high data rates for an FSR-UWB system with a frame time of $T_f = 40$ ns operating over the IEEE 802.15.4a office non-line-of-sight (NLOS) channel. The result “Analytical” uses the variance from (13), and the result “Without Frequency Offset” uses the variance from (13) with the $\cos(\cdot)$ terms removed (so that one can see the effects of the shift in frequency of the reference). Two results are apparent. First, the analytical result is accurate even for small values of N_f (which, per $R_b = 1/(N_f T_f)$, correspond to these high data rates). Second, depending on the error rate required, the frequency

offset of the reference starts to cause a loss in performance somewhere between 3.125 Mbits/s and 12.5 Mbits/s. Since the maximum excess delay spread of the IEEE 802.15.4a office NLOS channel is up to 150-200 ns, this matches our expectation that the FSR-UWB system performance will start to degrade when the system suffers appreciable intersymbol interference.

Next, the important comparison with TR-UWB is carefully considered. Recall that the motivation for the FSR-UWB system was one of reducing the receiver complexity of the TR-UWB system by removing the required delay line at the receiver, and thus performance even comparable to the TR-UWB system will make the FSR-UWB system attractive. Of course, any comparison is highly dependent upon the system constraints under which one is designing. Here, the data rate (and, hence, symbol period) and peak energy per pulse will be fixed for a given comparison. Then, the key parameter to be selected for each system is the number of frames per symbol N_f , which will then, of course, determine the frame time T_f . In standard TR-UWB systems, the number of frames per symbol (denoted $N_{f,TR}$) is often selected to avoid significant interpulse interference by guaranteeing that the interpulse spacing is greater than the root-mean-squared (RMS) delay spread of the channel [21]. Using an analogous rule for FSR-UWB, which requires only one pulse per frame, reveals that the FSR-UWB system will employ twice as many frames per symbol period to have roughly the same interpulse spacing as the TR-UWB system (i.e. $N_{f,FSR} = 2N_{f,TR}$). Initially, performance comparisons will be done under this rule. However, even this rule is somewhat arbitrary, because, in practice, one can continue to increase the average energy by increasing the number of frames (i.e. or reducing T_f) beyond where interframe interference (IFI) starts to degrade performance as long as such a degradation is offset by the increased average energy and the FCC spectral mask is not violated. A second round of comparisons will be made under this latter set of more pertinent constraints.

For the comparison where N_f is set to avoid significant interpulse interference, an interpretation of the analytic results developed above can be employed to roughly predict the results. In particular, as can be inferred from Figure 4, each of the systems will be dominated by the “noise cross noise” terms at the error rates generally of interest. Equations (16) and (17) then imply that, *if* the systems

employed equal N_f and an average energy constraint, the FSR-UWB system would exhibit a 1.5 dB gain. However, the FSR-UWB system will suffer a significant penalty under the peak power constraint due to the high peak-to-average power ratio (PAPR) of its pulses; in particular, its PAPR is 4.65 dB greater than that of the TR-UWB system. Combining these analytical results suggests approximately a 3.15 dB performance gain of TR-UWB over FSR-UWB under this set of assumed constraints (which will be subsequently modified).

Figure 6 shows performance results for the FSR-UWB and TR-UWB systems for various data rates on the IEEE 802.15.4a office NLOS channel under the assumption that the interpulse spacing is set to be larger than the RMS delay spread of the channel in each system. In particular, the frame length of the TR-UWB system is fixed at 32.25ns, and, per above, the frame length of the FSR-UWB system is one-half of such. The delay element of the TR-UWB is set to $D = 13.5$ ns. From these results, it is observed that the TR-UWB system outperforms the proposed system by somewhat less than the anticipated 3.15 dB under this peak power constraint. The difference can be attributed to the increased robustness of the FSR-UWB system to the small amount of IFI experienced, as will be observed more clearly in succeeding results. The gap between the two systems widens with increased data rate as the FSR-UWB system's performance degrades as the data rate approaches the inverse of the delay spread of the channel, as expected from Figure 5. Figure 7 shows analogous results for the IEEE 802.15.4a outdoor line-of-sight (LOS) channel. In this case, the frame length of the TR-UWB system is fixed at 62.5ns, and the frame length of the FSR-UWB system is 31.25ns. The delay element of the TR-UWB system is set to $D = 30$ ns. The conclusions from Figure 7 are similar to those drawn from Figure 6, except that the performance of the FSR-UWB system degrades more quickly with data rate due to the smaller coherence frequency of the outdoor LOS channel versus the indoor NLOS channel. This trend is further confirmed, as expected, on the IEEE 802.15.4a outdoor NLOS channel (not shown). Thus, the overall conclusion from this first set of comparisons is that the performance of the FSR-UWB system is reasonably comparable at low to moderate data rates to that of the TR-UWB system, as desired.

Above, we enforced the somewhat arbitrary constraint that the frame length (or, equivalently,

the number of frames N_f) be set such that there is limited interframe interference in each system. Here, such a constraint is removed to obtain a more pertinent comparison. In practice, N_f can be increased until either: (1) the gains from the increased average energy are offset by the degradation due to interframe interference, or (2) the FCC spectral limit is reached. Figure 8 displays the bit error probability versus peak pulse power to noise ratio (E_p/N_0) for the FSR-UWB system and TR-UWB system operating over an IEEE 802.15.4a office NLOS multipath fading channel for a fixed data rate (corresponding to a fixed $T_s = N_f T_f$) of 1 Mbits/sec. The delay element D is always set to be $2/5$ of the frame length in the TR-UWB system. The FSR-UWB system is more tolerant of IFI, and thus, if each system is allowed to employ an arbitrary N_f , the FSR-UWB system would continue to increase N_f to improve average energy aggregation and demonstrate a significant gain over TR-UWB. However, in practice, each of the systems is limited to the FCC mask, which translates here to an average energy constraint, and, hence, a limit on N_f . For a given E_p , the peak-to-average ratio and single pulse per frame of FSR-UWB implies that it employs 7.65 dB less average energy at a given peak energy than the TR-UWB system. Stated differently, this implies that, at the FCC constraint, $N_{f,FSR} = 5.83N_{f,TR}$. As an example, if the FCC constraint implies that $N_{f,TR} \leq 10$, then $N_{f,FSR} \leq 58$, and we can roughly compare the $N_{f,TR} = 10$ and $N_{f,FSR} = 60$ curves of Figure 8. Over a wide range of error probabilities and constraints, a 1.0 dB to 1.5 dB gain is observed for the FSR-UWB system. Figure 9 demonstrates analogous results for the IEEE 802.15.4a outdoor LOS multipath fading channel at a data rate of 1 Mbit/s.

Finally, the ability of FSR-UWB to withstand extreme Doppler shifts is tested. Extreme Doppler is simulated by changing both the environment and the channel independently once per *frame*. Results are shown in Figure 10, where System I and System II have 25 frames of length 50 ns and 20 ns, respectively. The environment has a number of paths that is uniformly distributed between 10 and 20, an interpath spacing that is uniformly distributed between 1 ns and 2 ns, and a decay constant $\bar{\tau}$ for an exponential decay profile that is uniformly distributed between 10 ns and 100 ns. Clearly, as with the TR-UWB system, the FSR-UWB system can be employed in systems with high mobility.

4.3 Discussion

Per the previous section, the FSR-UWB system not only obviates the need for the delay line in the TR-UWB system but also, in the targeted low data rate application area, provides a significant performance improvement. However, when viewing the selection of a wireless system technology more generally, the question of whether such a UWB system is preferable in practice to, say, a narrowband system, still arises. In particular, the performance of transmitted reference systems versus required average energy (e.g. see [12]) on any channel is greatly limited by the “noise cross noise terms,” and the significant reduction in the fading margin for UWB systems operating over multipath fading channels can be offset by this limitation.

Resolving the UWB system versus narrowband system debate is beyond the scope of this paper and will greatly depend on the application area of interest (e.g. UWB systems provide the capability for excellent localization), but we hasten to point out that there are significant enhancements that can be made to the FSR-UWB (or TR-UWB) system to improve performance that have not been considered here. In particular, a FSR-UWB scheme that employs multiple carriers has been demonstrated in [23], and it provides a significant performance improvement versus the baseline FSR-UWB scheme while still not requiring a delay line in the receiver. Another potential enhancement, particularly for AWGN channels or multipath channels with small delay spread, is to acquire frame timing so that the integration interval $[0, T_s]$ can be reduced to only those times for which the noiseless received signal has support.

5 Conclusions

In this paper, it has been shown that the need for a delay element in the receiver of a transmitted reference UWB system can be obviated by employing a data signal that is offset in frequency (rather than time) from the reference signal. By observing that the data signal and reference signal need only be orthogonal across the entire symbol period, the frequency offset can be chosen small enough to be well less than the coherence frequency of the channel in the targeted low to moderate data rate applications. A simple synchronization scheme also exists for the proffered system.

The scheme does not perform well in the presence of appreciable intersymbol interference, and, hence, is not suitable for high data rate systems that incur such. However, for the targeted low to moderate data rate applications, such an architecture not only greatly simplifies receiver design, but numerical results also indicate that the proposed scheme outperforms the standard TR-UWB scheme.

Acknowledgments

We are indebted to the participants in the UWB session at the 2004 Asilomar Conference on Signals, Systems, and Computers, whose active and frank discussion on the limitations of various forms of UWB receivers led to the motivation for this work that is described in the Introduction. Special thanks goes to Wesley Gifford of the Massachusetts Institute of Technology (MIT) for fruitful discussions regarding his Asilomar 2004 paper and for providing an advanced version of [18]. Robert Egri of M/A-COM, Inc., was the first to note the similarities in aspects of the proposed scheme to conventional amplitude modulation (AM). The three reviewers of the original manuscript provided feedback that has significantly improved the final paper; in particular, the detailed comments of the reviewers greatly improved the presentation of the simulation results and, most markedly, the comparison to the standard TR-UWB system.

A Noise Analysis of Proposed Scheme

In this appendix, the second moments of the “signal cross noise” and “noise cross noise” terms required in (8) are evaluated. The “signal cross noise” term can be evaluated as follows:

$$\begin{aligned}
& E \left[\left(2\sqrt{2} \int_0^{T_s} x(t)n(t) \cos(2\pi f_0 t) dt \right)^2 \right] \\
&= 4 \int_0^{T_s} \int_0^{T_s} E_s u(s)u(t) R_n(t-s) \cos(2\pi f_0 s) \cos(2\pi f_0 t) ds dt \\
&\quad + 8 \int_0^{T_s} \int_0^{T_s} E_s u(s)u(t) R_n(t-s) \cos^2(2\pi f_0 s) \cos^2(2\pi f_0 t) ds dt, \tag{26}
\end{aligned}$$

where $R_n(\tau)$ denotes the autocorrelation function of the wideband noise process $n(t)$.

Now, the first of the two terms in (26) is evaluated as:

$$\begin{aligned}
& 4 \int_0^{T_s} \int_0^{T_s} E_s u(s) u(t) R_n(t-s) \cos(2\pi f_0 s) \cos(2\pi f_0 t) ds dt \\
\stackrel{(1)}{=} & 4E_s \sum_{k=0}^{N_f-1} \int_0^{T_s} \int_0^{T_s} p(s-kT_f) p(t-kT_f) R_n(t-s) \cos(2\pi f_0 s) \cos(2\pi f_0 t) ds dt \\
\approx & 4E_s \sum_{k=0}^{N_f-1} \cos^2(2\pi f_0 kT_f) \int_0^{T_s} \int_0^{T_s} p(s-kT_f) p(t-kT_f) R_n(t-s) ds dt \\
\stackrel{(2)}{=} & 4E_s \sum_{k=0}^{N_f-1} \cos^2(2\pi f_0 kT_f) \int_0^{T_s} \int_0^{T_s} p(s) p(t) R_n(t-s) ds dt \\
\stackrel{(3)}{=} & 4E_s \sum_{k=0}^{N_f-1} \cos^2(2\pi f_0 kT_f) \int_0^{T_s} p(t) \int_{-\infty}^{\infty} P(f) S_n(f) e^{j2\pi ft} df dt \\
\stackrel{(4)}{=} & 4E_s \sum_{k=0}^{N_f-1} \cos^2(2\pi f_0 kT_f) \cdot \frac{1}{N_f} \frac{N_0}{2} \\
\approx & E_s N_0
\end{aligned} \tag{27}$$

where $\stackrel{(1)}{=}$ follows because the support of $R_n(\cdot)$, which is the autocorrelation of a wideband noise process, is far less than $T_f - T_p$, $\stackrel{(2)}{=}$ and $\stackrel{(3)}{=}$ follow because of the limited support of the autocorrelation function $R_n(\cdot)$ of the wideband process $n(t)$, and $\stackrel{(4)}{=}$ follows from Parseval's Theorem.

Similarly, the second of the two terms in (26) can be evaluated as:

$$8 \int_0^{T_s} \int_0^{T_s} E_s u(s) u(t) R_n(t-s) \cos^2(2\pi f_0 s) \cos^2(2\pi f_0 t) ds dt \approx \frac{3}{2} E_s N_0 \tag{28}$$

Finally, the “noise cross noise” term can be evaluated as:

$$\begin{aligned}
E \left[\left(\sqrt{2} \int_0^{T_s} n^2(t) \cos(2\pi f_0 t) dt \right)^2 \right] & \stackrel{(1)}{=} 2 \int_0^{T_s} \int_0^{T_s} R_n^2(0) \cos(2\pi f_0 s) \cos(2\pi f_0 t) ds dt \\
& \quad + 4 \int_0^{T_s} \int_0^{T_s} R_n^2(s-t) \cos(2\pi f_0 s) \cos(2\pi f_0 t) ds dt \\
\stackrel{(2)}{=} & 2R_n^2(0) \int_0^{T_s} \cos(2\pi f_0 s) ds \int_0^{T_s} \cos(2\pi f_0 t) dt \\
& \quad + 4 \int_0^{T_s} \int_0^{T_s} R_n^2(t-s) \cos^2(2\pi f_0 s) ds dt \\
= & 2 \int_0^{T_s} \int_0^{T_s} R_n^2(s-t) ds dt \\
& \quad + 2 \int_0^{T_s} \int_0^{T_s} R_n^2(s-t) \cos(4\pi f_0 (s-t+t)) ds dt \\
= & 2 \int_0^{T_s} \left(\int_{-u}^u R_n^2(v) dv \right) du
\end{aligned} \tag{29}$$

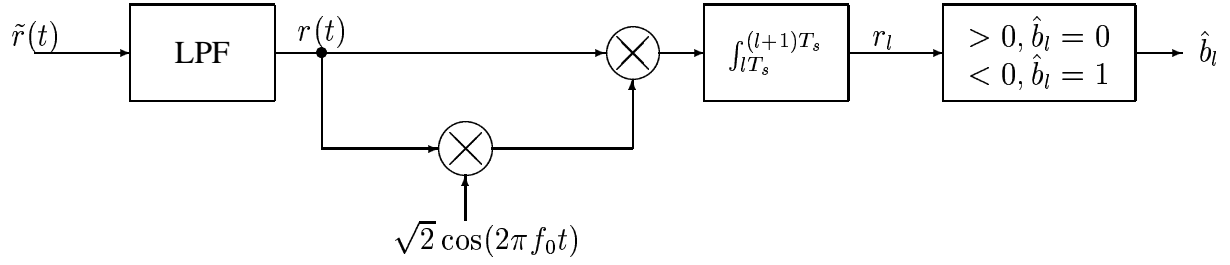
$$\begin{aligned}
& + 2 \int_0^{T_s} \left(\int_{-u}^u R_n^2(v) \cos(4\pi f_0 v) dv \right) \cos(4\pi f_0 u) du \\
& - 2 \int_0^{T_s} \left(\int_{-u}^u R_n^2(v) \sin(4\pi f_0 v) dv \right) \sin(4\pi f_0 u) du \\
\stackrel{(3)}{\approx} & 2 \int_0^{T_s} \left(\int_{-\infty}^{\infty} R_n^2(v) dv \right) du \\
& + 2 \int_0^{T_s} \left(\int_{-\infty}^{\infty} R_n^2(v) \cos(4\pi f_0 v) dv \right) \cos(4\pi f_0 u) du \\
& - 2 \int_0^{T_s} \left(\int_{-\infty}^{\infty} R_n^2(v) \sin(4\pi f_0 v) dv \right) \sin(4\pi f_0 u) du \\
\stackrel{(4)}{=} & T_s N_0^2 W \tag{30}
\end{aligned}$$

where $\stackrel{(1)}{=}$ comes from the standard decomposition of the expectation of the product of four Gaussian random variables, the second term in $\stackrel{(2)}{=}$ exploits the fact that the support of the autocorrelation function of the wideband noise is small enough that $\cos(2\pi f_0 t)$ does not change appreciably over it, $\stackrel{(3)}{\approx}$ exploits the fact that $R_n(\tau) \approx 0$ for $\tau \gg \frac{1}{W}$, and finally, Parseval's Theorem and the facts that $\int_0^{T_s} \cos(4\pi f_0 u) du = 0$ and $\int_0^{T_s} \sin(4\pi f_0 u) du = 0$ lead to $\stackrel{(4)}{=}$.

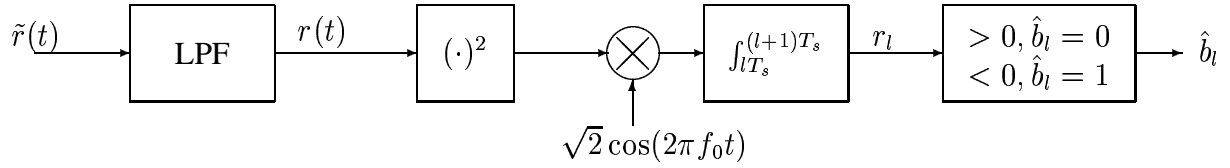
References

- [1] M. Win and R. Scholtz, "Ultra-wide Bandwidth Time-Hopping Spread-Spectrum Impulse Radio for Wireless Multiple Access Communications," *IEEE Transactions on Communications*, Vol. 48: pp. 679-691, April 2000.
- [2] R. Scholtz, D. Pozar, and W. Namgoong, "Ultra-Wideband Radio," *EURASIP Journal on Applied Signal Processing*, pp. 252-272, March 2005.
- [3] R. Wilson and R. Scholtz, "Comparison of CDMA and Modulation Schemes for UWB Radio in a Multipath Environment," *Proceedings of the Global Telecommunications Conference*, December 2003.
- [4] H. Sheng, R. You, and A. Haimovich, "Performance Analysis of Ultra-Wideband Rake Receivers with Channel Delay Estimation Errors," *Proceedings of the Conference on Information Sciences and Systems*, 2004.
- [5] A. Batra, J. Balakrishnan, G. Aiello, J. Foerster, and A. Dabak, "Design of a Multiband OFDM System for Realistic UWB Channel Environments," *IEEE Transactions on Microwave Theory and Techniques*, Vol. 52: pp. 2123-2138, September 2004.
- [6] R. Hoor and H. Tomlinson, "Delay-Hopped Transmitted-Reference RF Communications," *Proceedings of the IEEE Conference on Ultra-Wideband Systems and Technologies*, pp. 265-270, May 2002.
- [7] J. Choi and W. Stark, "Performance of Ultra-Wideband Communication with Suboptimal Receivers in Multipath Channels," *IEEE Journal on Selected Areas in Communications*, Vol. 20: pp. 1754-1766, December 2002.

- [8] M. Ho V. Somayazulu, J. Foerster, and S. Roy, "A Differential Detector for an Ultra-Wideband Communications System," *Proceedings of the IEEE Vehicular Technology Conference*, pp. 1896-1900, May 2002.
- [9] H. Zhang and D. Goeckel, "Generalized Transmitted-Reference UWB Systems," *Proceedings of the IEEE Conference on Ultra-Wideband Systems and Technologies (UWBST)*, November 2003.
- [10] Y. Chao and R. Scholtz, "Optimal and Suboptimal Receivers for Ultra-Wideband Transmitted Reference Systems," *Proceedings of the Global Telecommunications Conference*, December 2003.
- [11] S. Gezici, F. Tufvesson, and A. Molisch, "On the Performance of Transmitted-Reference Impulse Radio," *Proceeding of the 2004 Global Telecommunications Conference*, pp. 2874-2879, December 2004.
- [12] T. Quek and M. Win, "Analysis of UWB Transmitted-Reference Communication Systems in Dense Multipath Channels," *IEEE Journal on Selected Areas in Communications*, Vol. 23: pp. 1863-1874, September 2005.
- [13] L. Yang and G. Giannakis, "Timing Ultra-Wideband Signals with Dirty Templates," *IEEE Transactions on Communications*, Vol. 53: pp. 1952-1963, November 2005.
- [14] M. Casu and G. Durisi, "Implementation Aspects of a Transmitted-Reference UWB Receiver," *Wireless Communications and Mobile Computing*, Vol. 5: pp. 537-549, May 2005.
- [15] L. Feng and W. Namgoong, "An Oversampled Channelized UWB Receiver with Transmitted Reference Modulation," to appear in the *IEEE Transactions on Wireless Communications*.
- [16] S. Mitra, *Digital Signal Processing: A Computer-Based Approach*, McGraw-Hill, 1998.
- [17] N. van Stralen, A. Dentinger, K. Welles II, R. Gaus Jr., R. Hocter, and H. Tomlinson, "Delay Hopped Transmitted Reference Experimental Results," *Proceedings of the IEEE Conference on Ultra-Wideband Systems and Technologies (UWBST)*, May 2002.
- [18] W. Gifford and M. Win, "On Transmitted-Reference UWB Communications," Asilomar Conference on Signals, Systems, and Computers, 2004.
- [19] J. Proakis and M. Salehi, *Communication Systems Engineering*, Prentice-Hall, 1994.
- [20] S. Farahmand, X. Luo, and G. Giannakis, "Demodulation and Tracking with Dirty Templates for UWB Impulse Radio: Algorithms and Performance," *IEEE Transactions on Vehicular Technology*, Vol 54: pp. 1595-1608, September 2005.
- [21] Y. Chao and R. A. Scholtz, "Ultra-Wideband Transmitted Reference Systems," *IEEE Transactions on Vehicular Technology*, Vol. 54: pp. 1556-1569, September 2005.
- [22] IEEE 802.15 WPAN Low Rate Alternative PHY Task Group 4a (TG4a) 04/662r0, "Channel Model Final Report Revision 1", November 2004.
- [23] Q. Zhang and D. Goeckel, "Multi-Differential Slightly Frequency-Shifted Reference Ultra-Wideband (UWB) Radio," *Proceedings of the Conference on Information Sciences and Systems*, March 2006.



(a) FSR-UWB Receiver



(b) FSR-UWB Alternate Receiver

Figure 1: Receiver for the proposed FSR-UWB system. Note that the delay element of the standard TR-UWB scheme has been replaced by a mixer in (a). Since multiplication is commutative, the receiver in (a) can be drawn in the more convenient form given in (b).

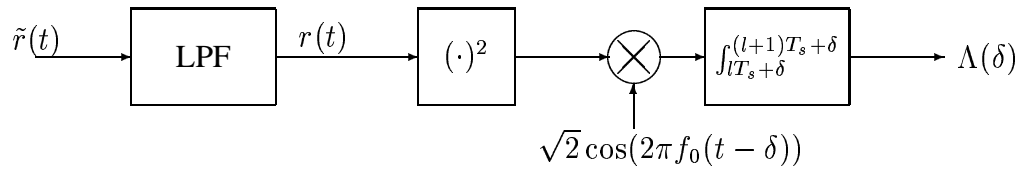


Figure 2: FSR-UWB receiver diagram showing the unknown time synchronization parameter δ .

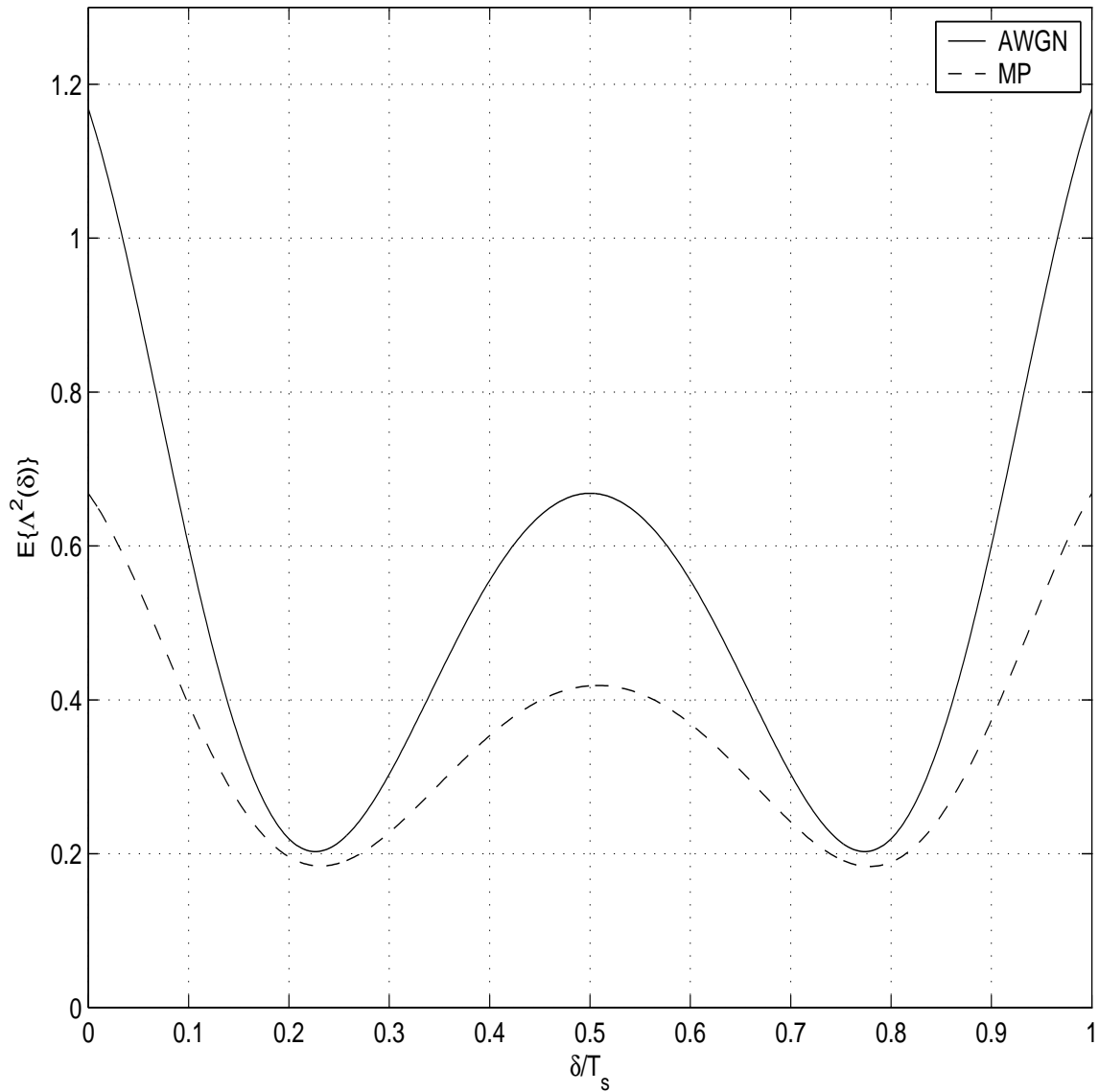


Figure 3: Proposed synchronization metric $E[\Lambda^2(\delta)]$ versus δ in normalized symbol periods for a system with parameters as given in the text. This figure indicates that the system can be synchronized by finding the δ that results in the maximum receiver output energy.

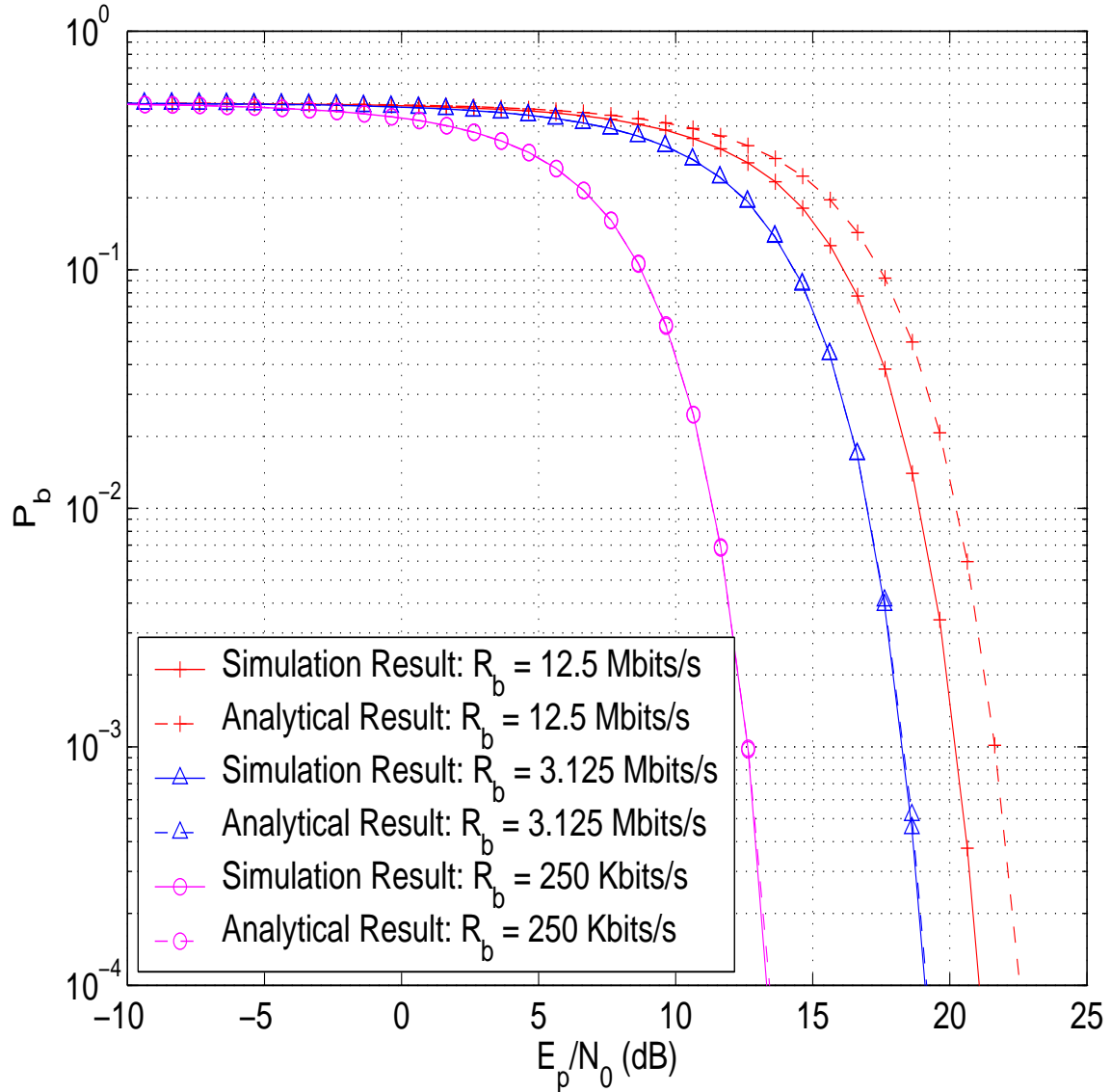


Figure 4: The bit error probability versus peak pulse energy to noise ratio (E_p/N_0) for the proposed FSR-UWB system with a fixed frame time of $T_f = 40$ ns (which, with R_b , determines N_f) operating on an AWGN channel. Solid lines represent simulation results, while the dashed-line curves represent analytical results from (10). For the simulation results, more than $\frac{100}{\hat{P}_b}$ data symbols have been run for each point, where \hat{P}_b is the displayed error probability estimate.

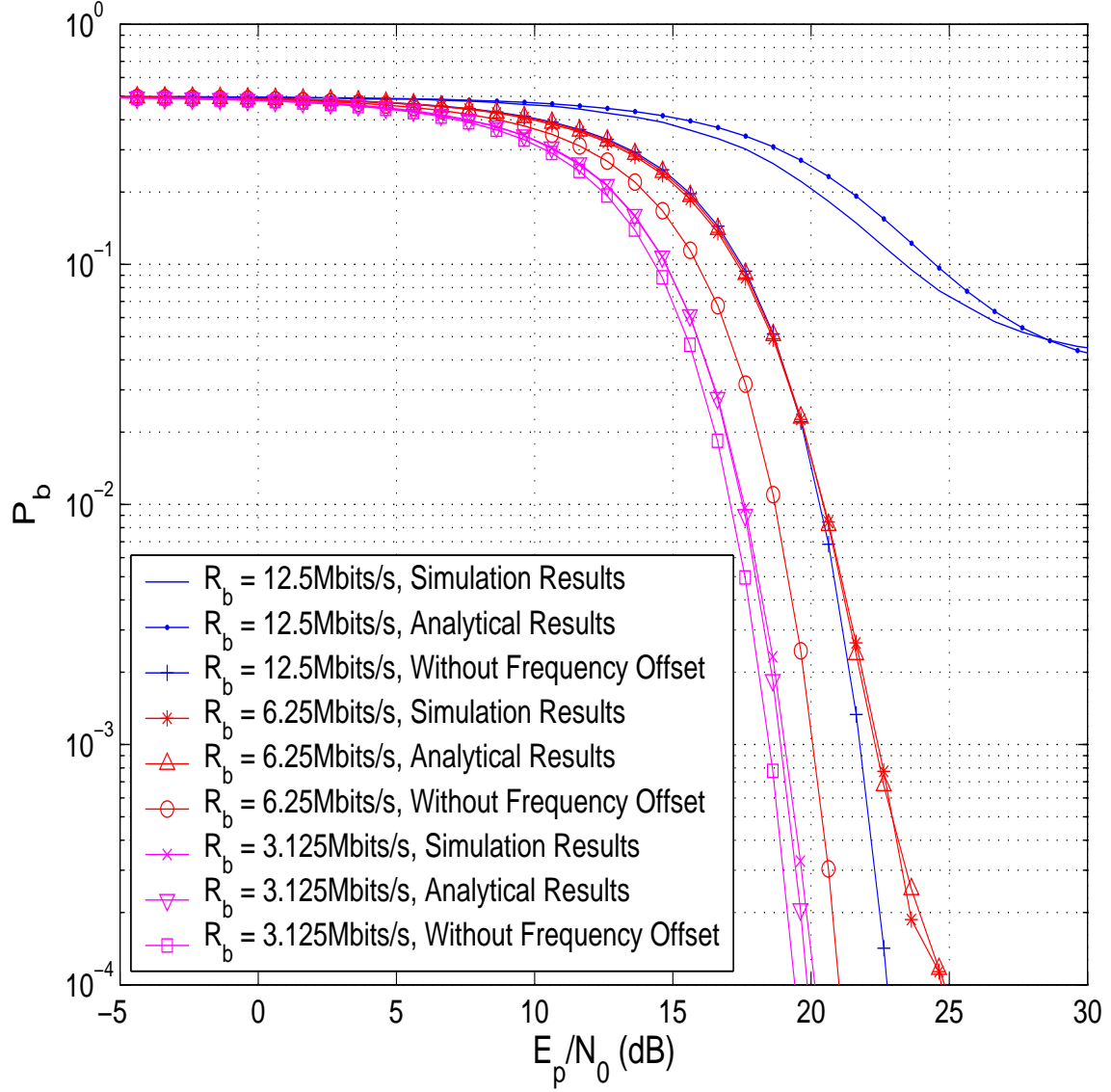


Figure 5: The bit error probability versus peak pulse energy to noise ratio (E_p/N_0) for the proposed FSR-UWB system with a fixed frame time of $T_f = 40$ ns (which, with R_b , determines N_f) operating over an IEEE 802.15.4a office NLOS multipath fading channel. For each analytic point, 10^5 random channels \underline{h} are generated to empirically estimate the required expectation.

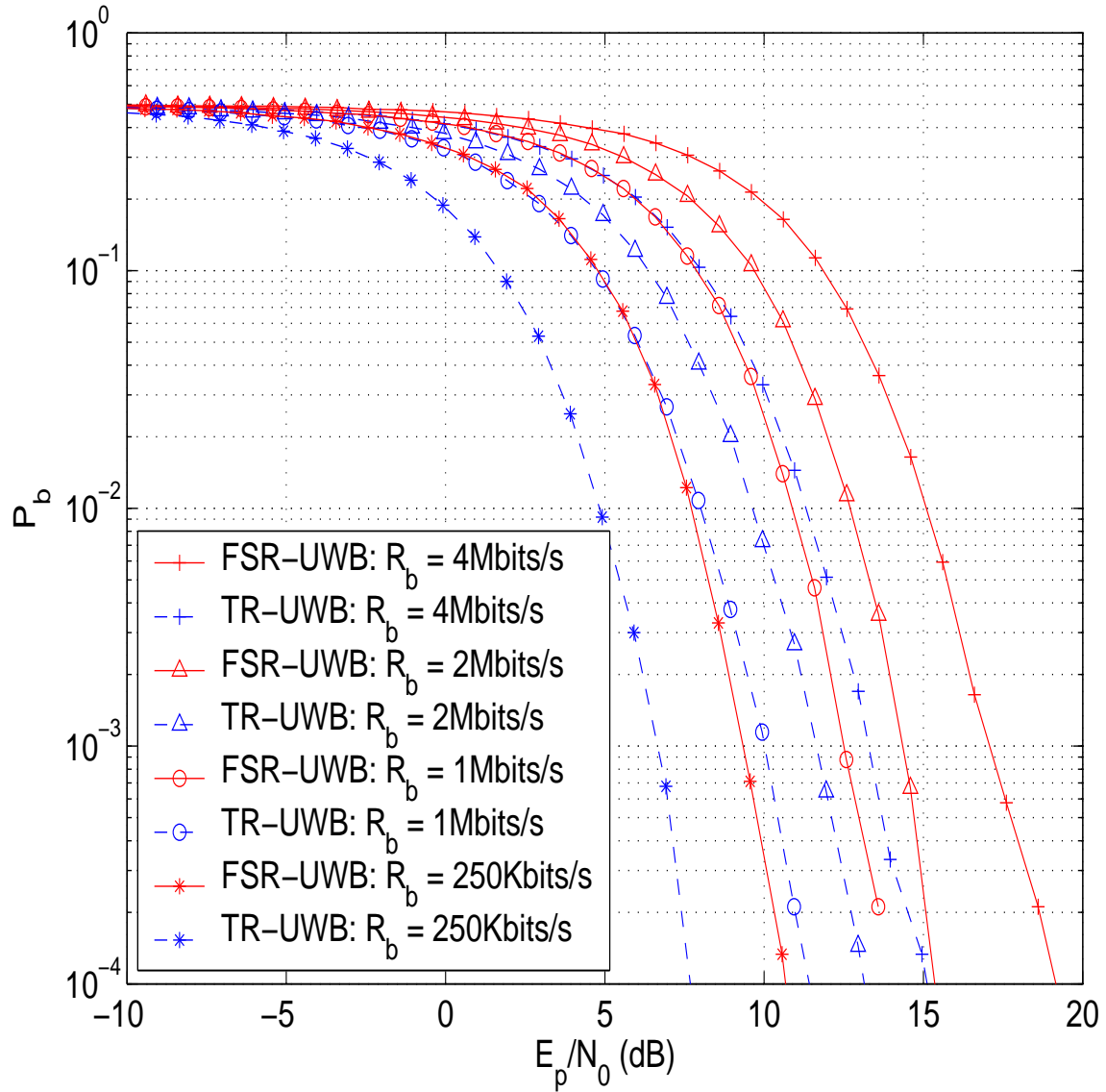


Figure 6: The bit error probability versus peak pulse energy to noise ratio (E_p/N_0) for the FSR-UWB system (solid curves) and TR-UWB system (dashed curves) operating over an IEEE 802.15.4a office NLOS multipath fading channel. In this case, N_f has been set (somewhat arbitrarily) for each system to avoid significant interpulse interference. For each point, 10^6 data symbols have been simulated. A comparison under more pertinent constraints for the same systems and channel is shown in Figure 8.

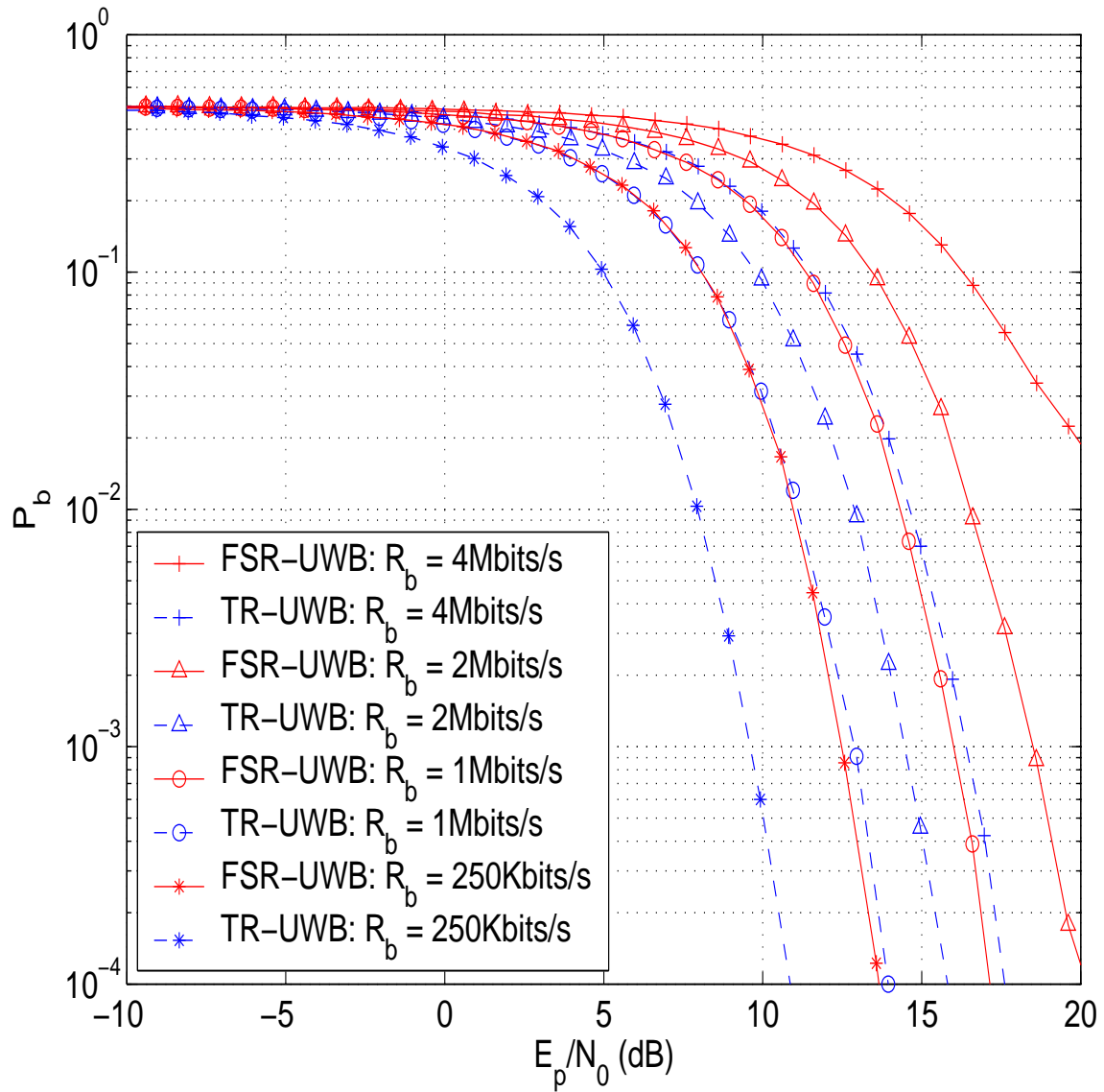


Figure 7: The bit error probability versus peak pulse energy to noise ratio (E_p/N_0) for the FSR-UWB system (solid curves) and TR-UWB system (dashed curves) operating over an IEEE 802.15.4a outdoor LOS multipath fading channel. In this case, N_f has been set (somewhat arbitrarily) for each system to avoid significant interpulse interference. For each point, 10^6 data symbols have been simulated. A comparison under more pertinent constraints for the same systems and channel is shown in Figure 9.

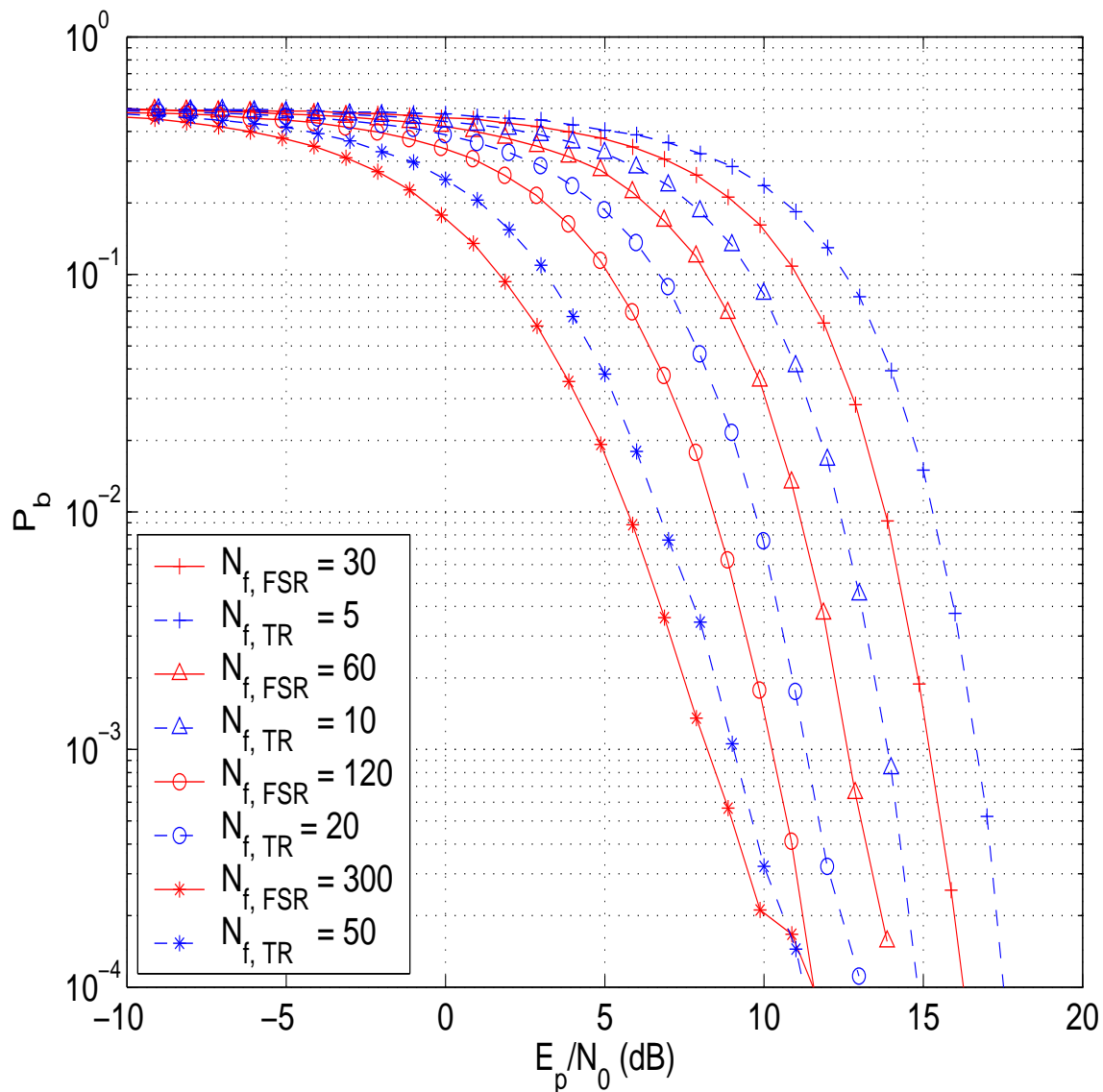


Figure 8: The bit error probability versus peak pulse energy to noise ratio (E_p/N_0) for the FSR-UWB system (solid curves) and TR-UWB system (dashed curves) operating over an IEEE 802.15.4a office NLOS multipath fading channel for a data rate of 1 Mbits/sec. For the simulation results, 10^6 data symbols have been run for each point. Per the text, $N_{f,FSR} \approx 6N_{f,TR}$ under the pertinent system constraints.

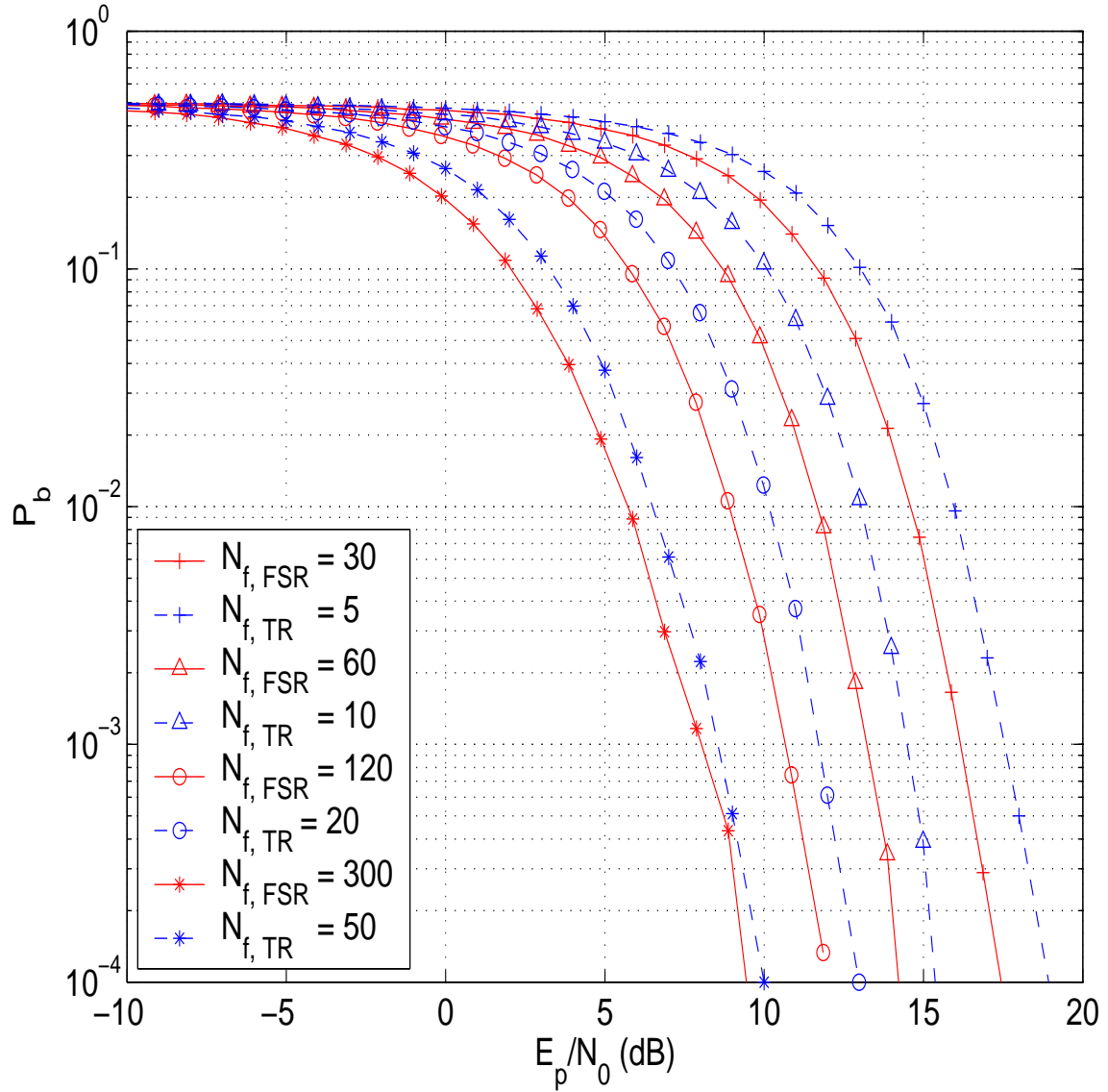


Figure 9: The bit error probability versus peak pulse energy to noise ratio (E_p/N_0) for the FSR-UWB system (solid curves) and TR-UWB system (dashed curves) operating over an IEEE 802.15.4a outdoor LOS multipath fading channel for a data rate of 1M bits/sec. For the simulation results, 10^6 data symbols have been run for each point. Per the text, $N_{f,FSR} \approx 6N_{f,TR}$ under the pertinent system constraints.

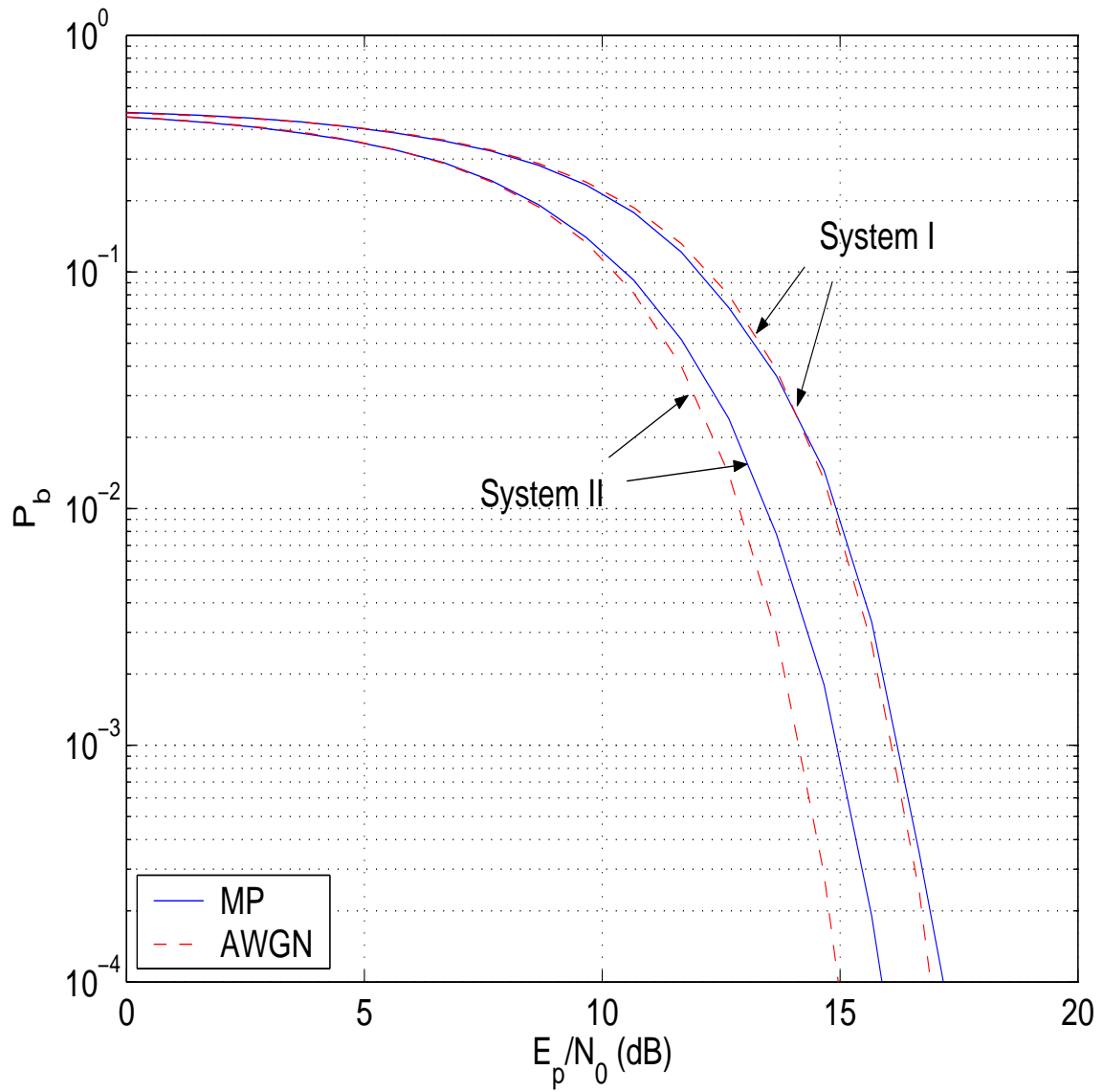


Figure 10: The bit error probability versus peak pulse energy to noise ratio (E_p/N_0) for the FSR-UWB system operating over a fast fading multipath channel. The multipath fading channel changes independently from frame to frame.